IEEE Areospace Conference Proceedings, Mar. 7 – 12, 2004, Paper # 5.0903

Synthetic Aperture Ladar Simulations with Phase Screens and Fourier Propagation[1,2]

Robert L. Lucke, Code 7218
U.S. Naval Research Laboratory
Washington DC 20375
(lucke@nrl.navy.mil, 202-767-2749)

Abstract—The ability to simulate the effect of turbulence on the phases and amplitudes of laser beams will aid the development of a practical synthetic aperture ladar (SAL). Simulations can obtain results in areas of interest that are resistant to theoretical investigation. Modeling turbulence with phase screens and using Fourier propagation can achieve the requisite simulation accuracy in reasonable computation time. Where possible, simulation results are compared to theoretical expectations. Tutorial information on generating random phase screens in a computationally efficient and conceptually simple way from a Kolmogorov (or any other) turbulence power spectrum is provided.

TABLE OF CONTENTS[1,2]

1. INTRODUCTION

The type of synthetic aperture ladar (SAL) discussed here is the exact optical analogy of synthetic aperture radar (SAR), and a reasonable degree of familiarity with SAL and SAR terminology and techniques is assumed. The interested reader is referred to Lucke and Rickard[1] for an introduction that serves as a lead-in to this topic, and/or to any of many SAR books[2,3]. In the past few years, some steps on the theory and practice of a practical SAL have taken place[1,4,5,6,7]. One of the most obvious impediments to such a system is the effect of atmospheric turbulence. Theoretical treatment of the impact of turbulence on SAL[7] is limited to the estimation of averages and does not extend reliably to the high-turbulence regime.

This paper describes a computer simulation of the effects of random realizations of turbulence. It is critical to any such simulation that both the phases and amplitudes of the transmitted and return beams be accurately reproduced so that the phase-sensitive heterodyne detection overlap integral can be accurately calculated. Other remote sensing laser applications do not require that phase be preserved. For example, coherent lidars are used to probe atmospheric constituents and use heterodyne detection as a sensitive means of measuring the return signal, but do not keep track of phase because the return comes from a substantial range of depths in the atmosphere, so that phase is averaged out. Thus the overlap integral in Belmonte's[8] Eq. (1) involves only beam intensities, not their phases and amplitudes.

Fried[9] considered heterodyne detection of a light beam that has been corrupted by passage through a turbulent atmosphere and derived the celebrated Fried parameter, r_0, that describes the diameter of a coherence patch of the atmosphere. The value of r_0 sets a point of diminishing returns on the physical aperture of an optical sensor (whether using a normal or heterodyne detector): increasing the aperture size beyond this point does not yield much improvement in signal or in resolution. Fried did not consider the phase-preserving part of optical heterodyne detection, but his results are applicable to SAL as far as they go. Karr[7] extended Fried's analysis to SAL and derived ρ_0, the equivalent of the Fried parameter for SAL. For the monostatic case (all that will be considered here), $\rho_0 = r_0/2^{6/5} = r_0/2.3$. So, from Eq. (6.13) of Fried,

$$\rho_0 = \frac{r_0}{2^{6/5}} = \frac{1.17\times10^{-8}}{2.30}\frac{\lambda_\mu^{6/5}}{\left(RC_n^2\right)^{3/5}} = 32\lambda_\mu^{6/5}\left[\frac{1\text{km}}{R}\right]^{3/5}\left[\frac{10^{-16}}{C_n^2}\right]^{3/5} \text{ cm}, \quad (1)$$

where λ_μ is the wavelength in microns, R is the range, and C_n^2 is the conventional descriptor of turbulence. Karr found that as the length of the synthetic aperture approaches and exceeds ρ_0, the resolution of the SAL stops improving. This paper supports Karr's assessment with the qualification that the term "resolution" as used by him is something of a misnomer. I will argue theoretically in Sec. 2 and show by simulation in Sec. 3 that Karr's measure of resolution actually measures a combination of resolution and contrast. The distinction between them is hard to make in Karr's theoretical analysis, but is readily apparent in simulations.

An effect of the atmosphere that certainly has the potential to harm SAL resolution is shot-to-shot piston variation over the beam footprint, where the "shot" referred to is from the

[1] U.S. Government work not protected by U.S. copyright.
[2] IEEEAC paper #1340, Final version, January 23, 2004.

laser that illuminates the scene. Piston effects are irrelevant to the basic problem considered by Fried of receiving a laser transmission, or to any lidar system that probes the atmosphere, but are potentially fatal to SAL. If turbulence is sufficiently high, these variations will disrupt the output of the phase-history matched filters used to form an image. But piston, by definition, is constant over the footprint for each shot, hence constitutes exactly the kind of error that SAR signal processing techniques have been developed to correct. I will show below that the same technique works for SAL, as expected, but it remains to be seen how well the technique can be applied in reality when the piston errors must be estimated from the scene, instead of being calculated in a simulation, and how far into turbulence the method can be pushed.

The well-known fact that a wave front tilt error displaces or distorts an image without degrading resolution applies also to SAL. When a monostatic SAL system transmits a pulse, atmospheric tilt of the wave front causes the beam to strike the ground at a point different from the aim point, but retro-reflected light then retraces its path to the receiver and is detected with no tilt-induced loss of efficiency.

2. DEFINITIONS OF RESOLUTION

I begin this discussion by noting that the proper description of a coherent imaging system is provided by its impulse response (IPR), while an incoherent system is described by its point spread function (PSF), which is the squared magnitude of the IPR. In SAR terminology, the squared magnitude is often referred to as the power IPR. The frequency response of a coherent system is the Fourier transform of the IPR, while that of an incoherent system is the Fourier transform of the PSF[10], which is the OTF (optical transfer function), and the magnitude of the OTF is the MTF (modulation transfer function). The definition of resolution for an optical system used by Karr is taken from Eq. (8.6-38) of Goodman[11] with different notation:

$$Res = \frac{1}{(2\pi)^2}\int \left\langle M(\vec{J})\right\rangle d\vec{J} \quad , \tag{2}$$

where $\vec{J}$ is a two-dimensional spatial-frequency variable, the brackets denote an ensemble average, and $M(\vec{J})$ is properly the OTF, but referred to by Karr as the MTF. Note that larger *Res* means better resolution. A more conventional definition of resolution is the full width at half maximum (FWHM) of the PSF. Smaller FWHM means better resolution. As discussed by Karr, turbulence does not affect the system in the range coordinate, so any degradation of resolution indicated by Eq. (2) applies to the azimuth coordinate. In this paper, I use FWHM in reference only to the azimuthal PSF, so, if Eq. (2) is a good measure of resolution, we expect to find that

$$\mathrm{FWHM} \propto \frac{1}{Res} \quad . \tag{3}$$

The FWHM of the PSF is determined primarily by the width of the region of support of the MTF, *i.e.*, by J_{max}, while the values of the MTF within that region determine contrast. In principle, contrast can be restored with image processing techniques that boost the value of the MTF, while loss of resolution due to a decrease in J_{max} is unrecoverable. (The distinction between resolution and contrast is readily apparent, and their dependence on the structure of the MTF can be easily explored, by analyzing the MTF of sparse aperture imaging systems, a subject to which the interested reader is referred[12].) Thus the definition of resolution given in Eq. (2) can be criticized on the grounds that it fails to distinguish between loss of resolution, as measured by FWHM, and loss of contrast. The integral in Eq. (2) might better be called a measure of image quality than of resolution.

Eq. (2) can also be criticized on the grounds that the MTF is derived from the PSF, not the IPR, hence is not appropriate for a coherent system. This criticism is mitigated by the fact that Karr develops expressions for the SAL MTF only to obtain the measure of resolution given in Eq. (2), not to describe the frequency response of the system.

3. THE SIMULATION: INPUTS AND RESULTS

This paper reports the simulation of the relatively simple case of a SAL operated from a low-altitude air-borne platform at a range of 10 km from the observed point on the ground. For this initial exercise, turbulence is constant along the light path, rather than given a different value at each phase screen. Monostatic, spotlight mode operation is simulated with 11 laser shots, spaced 2 cm apart. At a flight speed of 100 m/sec, this implies a synthetic aperture length of 20 cm, an imaging time of 2 ms, and a 5 KHz PRF. Turbulence is modeled with 5 phase screens, spaced 2 km apart, a spacing that easily satisfies the criterion set out in the Appendix [Eq. (A33)] for $C_n^2 \le 3\times10^{-16}$ m$^{-2/3}$. With these parameters and in the absence of turbulence, SA resolution exceeds the diffraction-limited resolution of the physical aperture by a factor of 10. A purely side-looking line of sight is assumed, but the simulation can accommodate a squint angle, if desired. An ideal flight path is assumed, but platform motion errors can be modeled by introducing the appropriate phase errors. The frequency chirp of the transmitted beam is not modeled: it is assumed that the deramp frequency from a given range is pure and immutable, uncorrupted by any effects of imperfect hardware. With the relatively small grid sizes used here (128×128), the simulation runs fast: the data for Figures 6 and 7, for examples, took less than 1 minute to create on a Pentium 4 machine.

Simulation parameters

$\lambda = 1.5\ \mu$	
$D = 4$ cm	physical aperture diameter
$w_o = 1.8$ cm	transmitted Gaussian beam waist
$L_{SA} = 20$ cm	synthetic aperture length
$R = 10$ km	range to scene
$F = 40$ cm	ground footprint diameter

Phase screen parameters (see Appendix)

$\Delta x = 1$ cm	grid sample spacing
$S = 1.28$ m	side of square column through atmos.
$K_L = 2\pi/S$	lowest DFT frequency
$K_H = 2\pi/(2\Delta x)$	highest DFT frequency
$K_O = 2\pi/(20\text{ m})$	turbulence outer scale frequency
$K_I = K_H$	turbulence inner scale frequency

The simulation begins with a Gaussian-profile beam of laser light with wavelength λ transmitted from an aperture of diameter $D = 2.25w_o$, where w_o is the initial Gaussian beam waist (this D/w_o ratio maximizes intensity at the center of the beam in the far field, for fixed D). The system is monostatic: the same aperture is used for reception. The beam immediately encounters a phase screen (see Appendix) and is then Fourier propagated[10,13] to the next phase screen. There are five phase screens, at 2-km intervals, with the ground 2 km beyond the last screen, for a total propagation distance of 10 km. (There is no need to put a screen at the ground because that would just make it part of the scene, which has phase-random reflectivity anyway.)

The beam illuminates a region on the ground – the "footprint" – and the phase and amplitude of this illumination at a point object in the footprint is recorded. Speckle can be simulated by assigning a random complex reflectivity to the object, but that is not done in this simulation. In reality, the light reflected from this point object would spread out spherically on its return to the receiver, but a wave front that propagates into 2π steradians cannot be modeled with Fourier propagation. Instead, its phase and amplitude are bestowed upon a second Gaussian beam that is launched from the object point and returned through the same set of phase screens to the receiver. The initial waist of this beam is chosen so that its wave front spreads out over an area considerably larger than the receiving aperture. This provides a means of modeling the effect of the atmosphere on the received part of the return wave. The part of the wave front intercepted by the receiving aperture is cut out, zero padded[14], and Fourier transformed to find the phase-and-amplitude distribution in the focal plane. The same operation is carried out on an assumed local oscillator beam that is also presented to the receiving aperture, and the heterodyne signal is calculated via

$$Sig = \int_{A_d} E_{LO}^{*} E_{Ret}\, dxdy \quad , \tag{4}$$

where *LO* = local oscillator, *Ret* = return, and the integral is over the area of a detector. Eq. (4) describes the return from one range resolution element in the footprint, *i.e.*, in one frequency band in the output of the detector. If the signal for another range element is desired, an object (or objects) can be placed at the appropriate point(s) in the footprint and the simulation repeated.

Spotlight-mode operation is simulated by imposing 2 cm of relative motion between the platform and the first phase screen between shots of the laser. Phase screens closer to the target are shifted by proportionately smaller amounts and the footprint on the ground does not move. The range is kept constant, so flight along a curved path is simulated. (The simulator can easily accommodate a different path by the appropriate phase corrections.)

Figure 1 (next page) shows beam amplitude at the ground for the case of no turbulence. I plot amplitude, not intensity, because that is what determines the measured signal. Figure 2 shows the effect of the indicated turbulence level: substantial fluctuations in amplitude are present. The phase of the wave front whose amplitude is depicted in Fig. 1 is a perfect paraboloid and is shown as the dotted line in Figure 3. The phase of the wave front from Fig. 2 is shown as the solid line, and can be seen to be disturbed by the atmosphere. The dotted line has been displaced by a piston term so that the phases at the center of the figure are the same. Observe that the shape of the two curves is nearly the same: the main difference is that the curvature of the disturbed beam is slightly less than that of the undisturbed beam. This is due to the combined effects of the large-scale focus (quadratic) component of the atmosphere [Eq. (A26)] and of the local quadratic properties of the screens (see Figure A1). Higher-frequency phase errors, readily visible near the center of Fig. 3, are small. Fig. 3 shows that, after piston and tilt, the dominant effect of the atmosphere on the wave front is an overall quadratic term which acts to change the curvature of the wave front. The knowledge that the dominate phase errors caused by turbulence are of this type should be of considerable use in the development of SAL focusing algorithms.

It is surprising that the substantial amplitude fluctuations of Fig. 2 are accompanied by the rather benign phase disturbances of Fig. 3. Physical insight into the reason why phase is more robust than amplitude in the presence of turbulence can be gained by examination of Figure 4. If we assume that passage through the atmosphere adds a complex error term that has half the amplitude of the undisturbed field, then the amplitude can be increased by a factor of 1.5 if the error adds constructively and reduced by factor of 2 if it adds destructively, but the maximum phase error that can be introduced is only 30°. It is well known in SAR signal processing that phase errors of 30° or less do not substantially degrade an image. Amplitude variations of $\times 1.5$, $\div 2$, imply intensity variations of $\times 2.25$, $\div 4$, and it is intensity variations that are considered in the assessment of

turbulence effects on most systems. But SAL depends on phase and amplitude, especially phase, and may therefore be less disrupted by turbulence than experience with other systems might suggest.

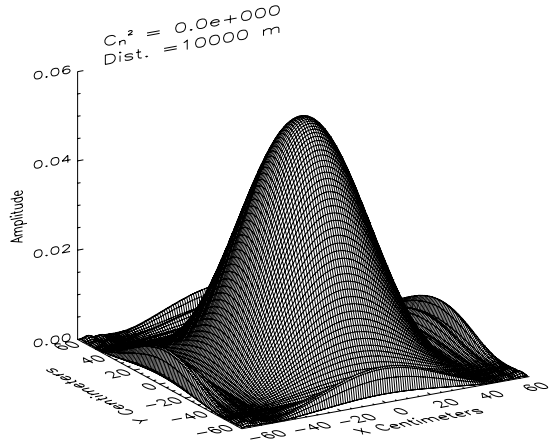

Figure 1. Laser beam amplitude (not intensity), shown relative to unity at the center of the transmitting aperture, on a surface that is perpendicular to the beam, at a distance of 10 km for zero turbulence. The central part of the beam, defined by $-20 \le x, y \le 20$, is one resolution element of the physical aperture and is used as the beam footprint for SAL simulations.

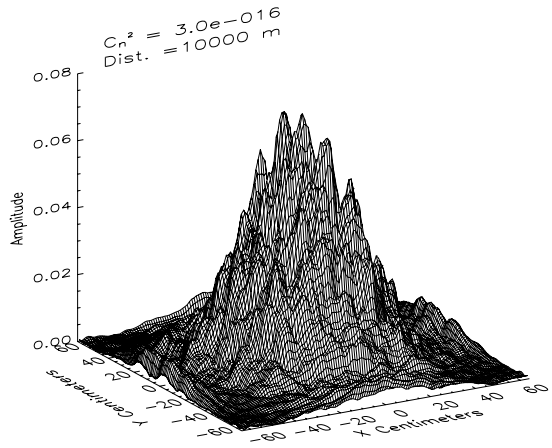

Figure 2. Same as Fig. 1, but with the indicated turbulence. Amplitudes generally differ from Fig. 1 by factors of 2 or less.

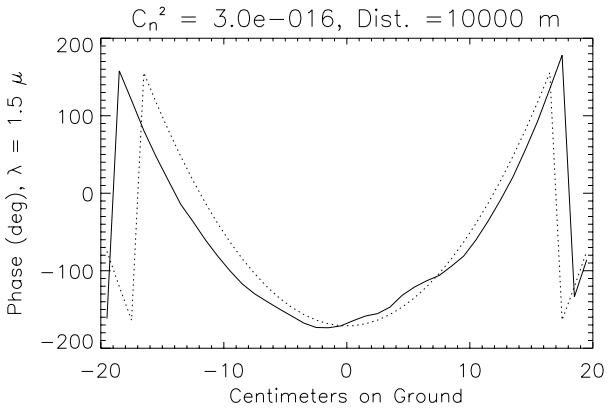

Figure 3. The wave front phases from Fig. 1 (dotted line) and Fig. 2 (solid line). A piston term has been added to the dotted line so that the lines match at the center.

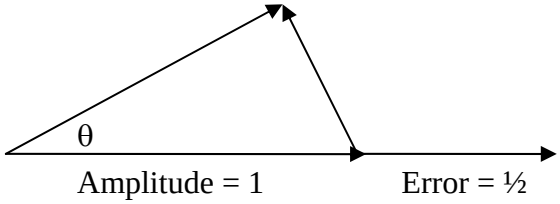

Figure 4. An error of ½ in amplitude can multiply amplitude by 1.5 if it adds constructively and by 0.5 if it adds destructively (not shown), but can introduce a phase error of no more than $\theta = \sin^{-1}(½) = 30°$.

The simulation proceeds by firing eleven laser shots, in the absence of turbulence, from flight positions separated by 2 cm, covering a synthetic aperture of 20 cm, with the signal from each shot calculated via Eq. (4). This is done for a point target at the center of the scene, then for a point target 1 cm from the center, *etc*., until a footprint 40 cm across has been fully characterized. For each point target, the 11 signals from Eq. (4) are reciprocated to obtain the matched filter that will pick out an object at that point in the scene. The same shot sequence is then repeated with or without turbulence and the returned signals multiplied by each of the filters to obtain an amplitude image which is squared to yield an intensity image.

Figure 5 shows two such images: the power IPR for a point object at the center of the footprint in the absence of turbulence (dotted line) and the image of a scene composed of two point objects, one at 0 cm and one at 10 cm, for a fairly low level of turbulence (solid line). Observe that

resolution, as measured by the FWHM of the peaks, is virtually unaffected. This is expected from Karr's results because ρ_0 = 52 cm for this case, while the length of the synthetic aperture is L_{SA} = 20 cm. With a ratio L_{SA}/ρ_0 = 20/52 ≈ 0.4, Karr predicts a negligible loss of resolution. Contrast does suffer slightly, because the background is higher.

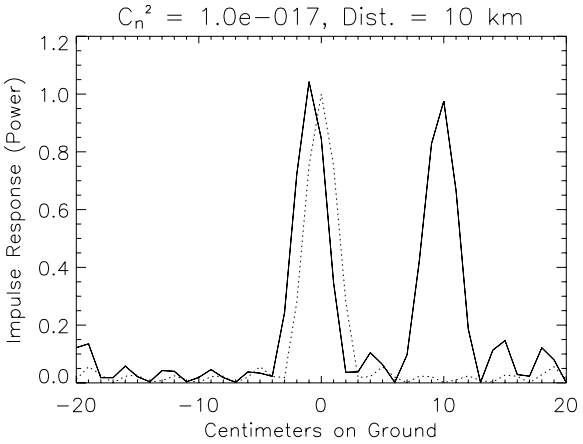

Figure 5. The dotted line is the power IPR (also known as the PSF) in the absence of turbulence for a point object at the center of the scene. The solid line is the image, after SA processing, but without phase correction, of a scene composed of two point objects, one at 0 cm and one at 10 cm. Observe that both peaks are displaced to the left by about 1 cm, showing that distortion (tilt) is nearly constant over the footprint.

Figure 6 shows an image of the same scene with fairly high turbulence; ρ_0 = 7 cm in this case and L_{SA}/ρ_0 = 2.9, for which Karr predicts a factor-of-three loss in resolution and Eq. (3) says that the same factor should apply to our FWHM. The combination of phase and amplitude errors have made the scene virtually unrecognizable, but the width of the peaks has not increased much, while contrast has suffered substantially. Thus, image quality is severely degraded, but *resolution* has not suffered much. With the simulator (as opposed to reality!) it is easy to keep track of the phase errors, and this was done for the object at the center. The phase corrections thus determined were then applied to the whole data set with the result shown in Figure 7: both objects now appear with essentially undiminished resolution and with much better contrast. That both objects have been recovered with the same phase correction shows that the phase errors are mostly constant across the footprint, exactly the case that SAR autofocus processing has been developed to handle. Methods of finding phase errors of this type from real data have received much attention for SAR and should be, to some extent at least, transferable to SAL. The heights of the peaks differ from unity because of the net effect of amplitude fluctuations in the signal. Unlike phase errors, net amplitude errors are not correctable because it is impossible to separate them from the unknown reflectivity of the object.

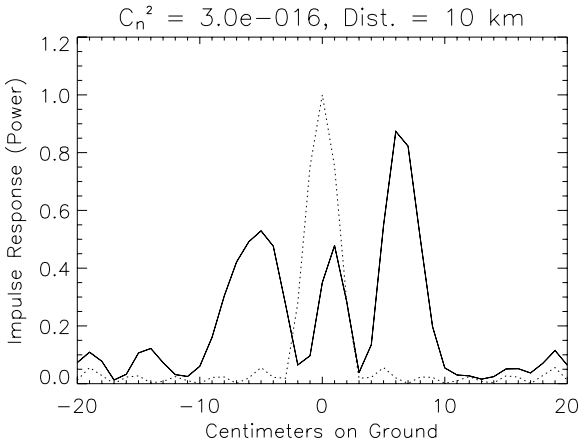

Figure 6. Same as Fig. 5, but at a higher level of turbulence.

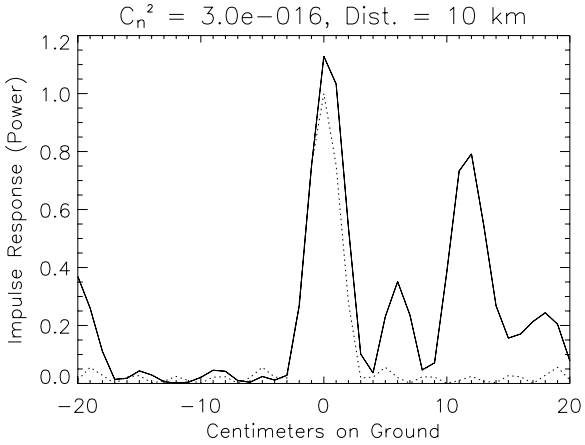

Figure 7. Data from Fig. 6, with phase correction applied. Observe that the separation between the peaks is about 11 cm, showing that some within-scene distortion is present.

4. CONCLUSION

The first results of a simulation of SAL performance have been presented. Future work includes an assessment of how phase screen parameters can be optimized to give good results in short computation times, with the primary aim of extending results to ranges up to 100 km. Preliminary investigation indicates that reducing the phase screen sample spacing below the 1 cm used here does not materially affect the results and that a larger spacing may be reasonable. Since the inner scale length of turbulence is rarely suggested to be smaller than a few mm, this seems reasonable. Also, the fewer phase screens that are used, the faster a simulation can run, so the criterion stated in Eq. (A33) needs thorough investigation.

Beyond these considerations, this simulation is ready to help address the engineering trade-offs necessary to the construction of a practical SAL. One of the most fundamental is the trade-off between 1.5 μ and 10 μ light. Eq. (1) shows that the coherence patch size of the atmosphere scales as $\lambda^{6/5}$, while, for the same resolution, the length of the synthetic aperture is proportional to λ. The trade-off ostensibly leaves 10 μ light with a $\lambda^{1/5}$ = 1.5 advantage. But how important is this advantage in the actual formation of images, especially when the improvements that can be implemented with signal processing are included? Simulations will strongly aid in answering this question.

Acknowledgement
This work was supported by the Defense Advanced Research Projects Agency.

APPENDIX: MODELING TURBULENCE WITH PHASE SCREENS

A1. Introduction: Modeling Low, Intermediate, and High Spatial Frequencies

The basic method of modeling propagation through the atmosphere is to sample the wave front on a square grid, apply a discrete Fourier transform (DFT) to obtain the wave's angular spectrum[10], propagate to a phase screen[11], inverse transform to obtain the amplitudes impinging on the screen, multiply by the phase change imposed by the screen, and repeat. The discussion here is on modeling the phase screen, which is done by generating a random turbulence spectrum in frequency space and inverse Fourier transforming to generate the phase screen in real space. Ideally, the screen would be large enough to include the outer scale of turbulence and its sampling would be fine enough to include the inner scale, but since the outer scale may be $10^{4\text{-}5}$ times the inner scale, arrays big enough to handle the entire range are impractical. The frequencies corresponding to the outer and inner scale lengths of turbulence, L_O and L_I, are $K_O = 2\pi/L_O$ and $K_I = 2\pi/L_I$. Using a grid with side S sampled at N points, the separation between points is $\Delta x = S/N$. The lowest frequency represented in this grid is $K_L = 2\pi/S$, and the highest is $K_H = 2\pi/(2\Delta x) = N\pi/S$. In the simulations reported here, Δx = 0.01 m, N = 128, and S =1.28 m. L_O is taken to be 20 m, so $K_O < K_L$. The primary effects of the low frequency range $K_O \le K < K_L$ are a large-scale tilt and focus of the wave front, which are modeled separately, as described in Sec. A3. At frequencies below K_O (most obviously the DC component) the power spectrum is set to zero. This simulation uses Δx = 1 cm, while L_I is generally a few mm, so $K_I > K_H$ and this high frequency range, $K_H < K \le K_I$, is neglected. The intermediate frequency range $K_L \le K \le K_H$ can be modeled directly [see Eq. (A7)]. The modeling methods for the different frequency ranges are summarized in Table 1.

Table A1.

Frequency Definition	Frequency Range	Phase Screen Modeled by
$K_O = 2\pi/L_O$ – Outer Scale Freq.	$K_O - K_L$	Tilt & Focus, Sec. A3
K_L, K_H – Low, High Freqs. of DFT	$K_L - K_H$	Eq. (A7)
$K_I = 2\pi/L_I$ – Inner Scale Freq.	$K_H - K_I$	Neglected

The contribution to the phase screen of the intermediate frequency range is derived in Sec. 2, the contribution of the low range in Sec. 3. Sec. 4 describes how the frequency components and tilt and focus contributions are randomized. Figure A1 (end of Appendix) shows a typical phase screen generated as described below and Figure A2 shows the phase structure function[9,15] associated with it. The structure function matches the theoretical prediction over the range of interest in this simulation, which has a beam footprint of 0.4 m, showing that the statistics of the phase screen are properly constructed.

A2. Intermediate Frequencies from a Randomized Turbulence Spectrum

Notation follows, though not strictly, that of Clifford[15]. Unless otherwise stated, λ is expressed in meters throughout this Appendix.

A phase screen models the phase change imposed on a wave front by an atmospheric volume V having length Z and area S^2 in the (x, y)-plane, centered on $(x, y) = (0, 0)$. In this simulation, Z = 2,000 m. The desired change in phase angle across the screen is

$$\alpha(x,y) = \frac{2\pi}{\lambda}\int_z n_1(x,y,z)dz \quad , \tag{A1}$$

where $n_1(x, y, z)$ is the variable part of the index of refraction. Our aim is to generate $\alpha(x, y)$. The autocorrelation of $n_1(x, y, z)$ is

$$\begin{aligned} B(x,y,z) &= \left\langle n_1(u+x,v+y,w+z)n_1(u,v,w)\right\rangle \\ &= \frac{1}{V}\iiint_V n_1(u+x,v+y,w+z)n_1(u,v,w)dudvdw \quad . \end{aligned} \tag{A2}$$

Also

$$B(x,y,z) = \iiint (2\pi)^3 \Phi_0(k_x,k_y,k_z) \times \exp\left[i(xk_x + yk_y + zk_z) \right] df_x df_y df_z \,, \tag{A3}$$

where the power spectrum of n_1 is written as $(2\pi)^3\Phi_0$ so that the Fourier transform variable is f instead of k. The power spectrum is non-zero only over the range $K_O \le K \le K_I$ where K is the magnitude of (k_x, k_y, k_z).

Now $(2\pi)^3\Phi_0 \equiv \langle \phi\phi^* \rangle$ where ϕ is the (properly randomized, see Sec. A4) spatial frequency spectrum of n_1. Eqs. (A2) and (A3) imply that

$$\frac{1}{V^{1/2}} n_1(x,y,z) = \iiint \phi(k_x,k_y,k_z) \exp\left[i(xk_x + yk_y + zk_z) \right] df_x df_y df_z \,, \tag{A4}$$

so

$$\phi(k_x,k_y,k_z) = \iiint \frac{n_1(x,y,z)}{V^{1/2}} \exp\left[-i(xk_x + yk_y + zk_z) \right] dx dy dz \,, \tag{A5}$$

and

$$\begin{aligned} \phi(k_x,k_y,0) &= \iint \int_z \frac{n_1(x,y,z)}{V^{1/2}} dz \exp\left[-i(xk_x + yk_y) \right] dx dy \\ &= \iint \frac{\lambda}{2\pi} \frac{\alpha(x,y)}{V^{1/2}} \exp\left[-i(xk_x + yk_y) \right] dx dy \quad , \end{aligned} \tag{A6}$$

hence

$$\alpha(x,y) = \frac{2\pi}{\lambda} V^{1/2} \iint \phi(k_x,k_y,0) \exp\left[i(xk_x + yk_y) \right] df_x df_y \,. \tag{A7}$$

Since α is real, ϕ must be Hermitian: $\phi(-k_x, -k_y) = \phi^*(k_x, k_y)$, a minor constraint on the randomization process described in Sec. A4. When implemented as a DFT, the integral in Eq. (A7) covers only the range $K_L \le K \le K_H$.

Eq. (A7) and Parseval's relation can be used to find the contribution to the mean square phase of any desired part of the power spectrum. The total mean square phase is

$$\left\langle \iint \alpha^2 dx dy \right\rangle = S^2 \left\langle \alpha^2 \right\rangle = \left\langle \left(\frac{2\pi}{\lambda} \right)^2 V \iint \phi\phi^* df_x df_y \right\rangle = \left(\frac{2\pi}{\lambda} \right)^2 V \int_{K_O}^{K_I} (2\pi)^3 \Phi_0 \, 2\pi f df \,, \tag{A8}$$

so, taking $\Phi_0 = 0.033 C_n^2 K^{-11/3}$ from Clifford[15] (for example) and using $0.033 \approx 1/30$, the contribution to $\langle \alpha^2 \rangle$ from frequencies modeled by the DFT (lower frequencies are treated in Sec. A3) is

$$\begin{aligned} \left\langle \alpha^2 \right\rangle &= \frac{(2\pi)^4 Z}{\lambda^2} \int_{K_L}^{K_H} \frac{C_n^2}{30} K^{-11/3} K dK \\ &= \frac{(2\pi)^4 C_n^2 Z}{30\lambda^2} \int_{K_L}^{K_H} K^{-8/3} dK \\ &= \frac{(2\pi)^4 C_n^2 Z}{30\lambda^2} \frac{3}{5} K^{-5/3} \Big|_{K_H}^{K_L} \\ &= \frac{(2\pi)^4 C_n^2 Z}{50\lambda^2} \left(\frac{1}{K_L^{5/3}} - \frac{1}{K_H^{5/3}} \right) \quad . \end{aligned} \tag{A9}$$

Thus the contribution to α_{rms} from intermediate frequencies is

$$\alpha_{IF,rms} = 0.382 \left(\frac{1\mu}{\lambda} \right) \left(\frac{Z}{1\text{km}} \right)^{1/2} \left(\frac{C_n^2}{10^{-16}} \right)^{1/2} \left(\frac{S}{1\text{m}} \right)^{5/6} \times \left[1 - \left(\frac{2\Delta x}{S} \right)^{5/3} \right]^{1/2} \text{ radians.} \tag{A10}$$

A3. Large-Scale Effects of Low Frequencies

If S is smaller than an outer scale length, frequencies lower than $K_L = 2\pi/S$ cannot be properly modeled with Eq. (A7) and a DFT. The effect of these frequencies is modeled analytically from the observation that most of the variation across a phase screen of a sinusoid with wavelength longer than the width of the screen is described by linear and quadratic terms. Another way to model these frequencies is to use segments of sinusoids that complete less than one cycle across the screen, with their amplitudes and phases randomized. This is implemented in Fourier space by Lane *et al*.[16], but could as easily and more straightforwardly be implemented in real space. The result is a structure function that follows the $r^{5/3}$ law over a broader range of r than shown in Fig. A2, but Fig. A2 shows that the $r^{5/3}$ law is well approximated over the range of interest in this simulation, which has a beam footprint of 0.4 m.

A3a. Linear Term ⇒ Tilt

The primary effect of the disturbance function ϕ for these frequencies is a constant tilt across the wave front. For a phase tilt inclined to the x axis, we write $a = \partial\alpha/\partial x$ so that $\alpha(x) = ax$ is the phase change imposed by the screen. [At $x = S/2$, the phase change is $\alpha = aS/2$, which means that the wave front is advanced by the distance $\Delta z = \alpha\lambda/2\pi = aS\lambda/4\pi$, which means that the angular tilt of the wave front is $\Delta z/(S/2) = a\lambda/2\pi$.] It follows from Eq. (A7) that

$$\frac{\partial \alpha}{\partial x} = \frac{2\pi}{\lambda} V^{1/2} \iint i k_x \phi(k_x, k_y, 0) \exp\left[i(x k_x + y k_y) \right] df_x df_y \ , \tag{A11}$$

so, from Parseval's relation,

$$\left\langle \iint \left[\left(\frac{\partial \alpha}{\partial x} \right)^2 + \left(\frac{\partial \alpha}{\partial y} \right)^2 \right] dx dy \right\rangle = \left\langle \left(\frac{2\pi}{\lambda} \right)^2 V \iint \left(k_x^2 + k_y^2 \right) \phi \phi^* df_x df_y \right\rangle . \tag{A12}$$

Redefining a by $a^2 \equiv (\partial\alpha/\partial x)^2 + (\partial\alpha/\partial y)^2$, Eq. (A12) becomes

$$S^2 \left\langle a^2 \right\rangle = \left(\frac{2\pi}{\lambda} \right)^2 V \int_{K_O}^{K_I} K^2 \, 2\pi \Phi_0 \, 2\pi K dK \ . \tag{A13}$$

The contribution to mean square tilt from frequencies below K_L is therefore given by

$$\left\langle a^2 \right\rangle_{K<K_L} = \frac{(2\pi)^4 Z}{\lambda^2} \int_{K_O}^{K_L} \frac{C_n^2}{30} K^{-11/3} K^3 dK = \frac{(2\pi)^4 C_n^2 Z}{10\lambda^2} \left(K_L^{1/3} - K_O^{1/3} \right) \ , \tag{A14}$$

and

$$a_{rms} = 5.36 \left(\frac{1\mu}{\lambda} \right) \left(\frac{Z}{1\ \mathrm{km}} \right)^{1/2} \left(\frac{C_n^2}{10^{-16}} \right)^{1/2} \left(\frac{1\mathrm{m}}{S} \right)^{1/6} \times \left[1 - \left(\frac{S}{L_O} \right)^{1/3} \right]^{1/2} \frac{\text{radians}}{\text{meter}} . \tag{A15}$$

Taking $\langle a^2 \rangle$ from Eq. (A14), a particular realization of a, denoted a_R, is obtained by randomizing amplitude according to Eq. (A30) (below) with $|\phi|$ replaced by a and $(2\pi)^3\Phi_0$ replaced by $\langle a^2 \rangle$. The azimuthal orientation of the tilt is chosen as an angle θ, random over $(0, 2\pi)$, so that the phase added to the screen is

$$\alpha_{tilt}(x, y) = a_R x \cos\theta + a_R y \sin\theta \ . \tag{A16}$$

Now, $\alpha_{tilt,rms} = (\langle a^2 \rangle S^2/12)^{1/2}$, so, from Eq. (A15),

$$\alpha_{tilt,rms} = 1.55 \left(\frac{1\mu}{\lambda} \right) \left(\frac{Z}{1\mathrm{km}} \right)^{1/2} \left(\frac{C_n^2}{10^{-16}} \right)^{1/2} \left(\frac{S}{1\mathrm{m}} \right)^{5/6} \times \left[1 - \left(\frac{S}{L_O} \right)^{1/3} \right]^{1/2} \text{radians} = 4.06 \left[1 - \left(\frac{S}{L_O} \right)^{1/3} \right]^{1/2} \alpha_{IF,rms} \ . \tag{A17}$$

Eq. (A17) states the rms phase angle due to tilt of the wave front, averaged over the square of side S. The rms phase angle due to local tilt of the wave front at a single sample point can be found by neglecting K_O in Eq. (A14) and replacing K_L by $\mathrm{Min}(K_H, K_I) = 2\pi/\mathrm{Max}(2\Delta x, L_I)$ to find

$$a_{sample,rms} = \frac{2\pi}{\lambda} \left[\frac{(2\pi)^{7/3} C_n^2 Z}{10 \mathrm{Max}(2\Delta x, L_I)^{1/3}} \right]^{1/2} \frac{\text{radians}}{\text{meter}} . \tag{A18}$$

Now, $\alpha_{sample,rms} = (\langle a^2 \rangle \Delta x^2/12)^{1/2}$ and we need $\alpha_{sample,rms} \le 2\pi/14$ in order that the sampling error be diffraction limited, so from Eq. (A18)

$$\frac{2\pi}{\lambda} \left[\frac{(2\pi)^{7/3} C_n^2 Z}{10 \mathrm{Max}(2\Delta x, L_I)^{1/3}} \right]^{1/2} \frac{\Delta x}{\sqrt{12}} \le \frac{2\pi}{14} \ , \tag{A19}$$

or

$$\Delta x \le \lambda \left[\frac{\mathrm{Max}(2\Delta x, L_I)^{1/3}}{119 C_n^2 Z} \right]^{1/2} \approx \frac{\lambda}{24 \sqrt{C_n^2 Z}} \ , \tag{A20}$$

which is a condition that the sampling interval, Δx, must satisfy, where the Max function has been replaced by 0.01 m in the last approximation: since the final expression depends only on the sixth root of this value, the approximation 0.01 m should be adequate in all cases of interest.

A3b. Quadratic Term ⇒ Focus

The contribution of low frequencies can be refined by adding quadratic effects, for which we write $b_x = \partial^2\alpha/\partial x^2$ so that $\alpha(x) = \frac{1}{2} b_x x^2$ is the phase change imposed by the screen. It follows from Eq. (A7) that

$$\frac{\partial^2 \alpha}{\partial x^2} = \frac{2\pi}{\lambda} V^{1/2} \iint -k_x^2 \phi(k_x, k_y, 0) \exp\left[i(x k_x + y k_y) \right] df_x df_y \ , \tag{A21}$$

so, from Parseval's relation,

$$\left\langle \iint \left(\frac{\partial^2 \alpha}{\partial x^2} \right)^2 dxdy \right\rangle = \left\langle \left(\frac{2\pi}{\lambda} \right)^2 V \iint k_x^4 \phi\phi^* df_x df_y \right\rangle$$
$$= \left\langle \left(\frac{2\pi}{\lambda} \right)^2 V \iint K^4 \cos^4\theta \, \phi\phi^* df_x df_y \right\rangle \qquad \text{(A22)}$$
$$= \left\langle \left(\frac{2\pi}{\lambda} \right)^2 V \iint \frac{3}{8} K^4 2\pi\Phi_0 \, 2\pi K dK \right\rangle \ ,$$

since the average value of $\cos^4\theta$ is 3/8. The quadratic contribution from frequencies below K_L is therefore

$$\left\langle b_x^2 \right\rangle_{K<K_L} = \frac{(2\pi)^4 Z}{\lambda^2} \int_{K_O}^{K_L} \frac{C_n^2}{80} K^{-11/3} K^5 dK$$
$$= \frac{(2\pi)^4 C_n^2 Z}{80\lambda^2} \frac{3}{7} \left(K_L^{7/3} - K_O^{7/3} \right) \qquad \text{(A23)}$$
$$= \frac{(2\pi)^4 C_n^2 Z}{187\lambda^2} \left(K_L^{7/3} - K_O^{7/3} \right) \ ,$$

and

$$b_{x,rms} = 7.8 \left(\frac{1\mu}{\lambda} \right) \left(\frac{Z}{1\,\text{km}} \right)^{1/2} \left(\frac{C_n^2}{10^{-16}} \right)^{1/2} \left(\frac{1\text{m}}{S} \right)^{7/6} \times \left[1 - \left(\frac{S}{L_O} \right)^{7/3} \right]^{1/2} \frac{\text{radians}}{\text{meter}^2} \ . \qquad \text{(A24)}$$

Similar expressions can be written for $b_y = \partial^2\alpha/\partial y^2$, and b_x and b_y are combined into $b_r = (b_x^2 + b_y^2)^{1/2}$, so $b_{r,rms} = 2^{1/2} b_{x,rms}$. A particular realization of b_r, denoted b_R, is randomized as was a_R above. Next, a random angle β is chosen to generate $b_{Rx} = b_R\cos\beta$ and $b_{Ry} = b_R\sin\beta$. Note that b_{Rx} and b_{Ry} can have opposite signs. Finally, the orientation of the quadratic function is again chosen as a random angle θ, so that the phase added to the screen for focus is

$$\alpha_{foc}(x,y) = \frac{1}{2} b_{Rx} (x\cos\theta + y\sin\theta)^2 + \frac{1}{2} b_{Ry} (-x\sin\theta + y\cos\theta)^2 - \frac{(b_{Rx} + b_{Ry}) S^2}{24} \ , \qquad \text{(A25)}$$

where the last term removes piston. Now, $\alpha_{foc,rms} = (\langle b_{Rx}^2 + b_{Ry}^2 \rangle S^4/720)^{1/2}$ so, from Eq. (A24),

$$\alpha_{foc,rms} = 0.41 \left(\frac{1\mu}{\lambda} \right) \left(\frac{Z}{1\text{km}} \right)^{1/2} \left(\frac{C_n^2}{10^{-16}} \right)^{1/2} \left(\frac{S}{1\text{m}} \right)^{5/6} \times \left[1 - \left(\frac{S}{L_O} \right)^{7/3} \right]^{1/2} \text{radians} \qquad \text{(A26)}$$
$$= 1.08 \left[1 - \left(\frac{S}{L_O} \right)^{7/3} \right]^{1/2} \alpha_{IF,rms} \ .$$

A4. Randomizing the Turbulence Spectrum

The central limit theorem decrees that, for any particular (k_x, k_y), $\phi(k_x, k_y, 0)$, must be a complex Gaussian random number, *i.e.*, has uniform distribution in phase and

$$P_{|\phi|}(|\phi|) = \frac{2|\phi|}{(2\pi)^3 \Phi_0} \exp\left[-\frac{|\phi|^2}{(2\pi)^3 \Phi_0} \right] \ . \qquad \text{(A27)}$$

Note that Φ_0 is the average of an exponential distribution:

$$P_\Phi(\Phi) = \frac{1}{\Phi_0} \exp(-\Phi/\Phi_0) \ , \qquad \text{(A28)}$$

where $(2\pi)^3\Phi = |\phi|^2$. A standard software package generates a random number x uniformly distributed over (0, 1), *i.e.*,

$$P_x(x) = 1 \ , \ 0 \le x \le 1 \ . \qquad \text{(A29)}$$

We set $\arg\phi = 2\pi(x - 0.5)$ to obtain a random $\arg\phi$ distributed uniformly over $(-\pi, \pi)$. Next we set $x = \exp[-|\phi|^2/(2\pi)^3\Phi_0]$ and solve for $|\phi|$,

$$|\phi| = \sqrt{-(2\pi)^3 \Phi_0 \ln(x)} \ , \qquad \text{(A30)}$$

to obtain a random $|\phi|$ distributed according to Eq. (A27). For the benefit of the suspicious reader, we observe from $x = \exp[-|\phi|^2/(2\pi)^3\Phi_0]$ and the fundamental relation $P(x)dx = P(|\phi|)(-d|\phi|)$ that

$$P_{|\phi|}(|\phi|) = P_x(x) \left(-\frac{dx}{d|\phi|} \right) = \frac{2|\phi|}{(2\pi)^3 \Phi_0} \exp\left[-\frac{|\phi|^2}{(2\pi)^3 \Phi_0} \right] \ , \qquad \text{(A31)}$$

as desired.

A5. Spacing the Screens

The normal rule for the maximum spacing between phase screens is that r_0, which is the diameter of a coherence patch of the atmosphere, should be at least as large as the diameter of the first Fresnel zone of one screen as seen from the next, that is,

$$r_0 = 1.17 \times 10^{-8} \frac{\left(10^6 \lambda\right)^{6/5}}{\left(Z C_n^2\right)^{3/5}} \ge 2\sqrt{\lambda Z} \ , \qquad \text{(A32)}$$

where Z is the distance between the screens. The first equality in Eq. (A32) is Eq. (6.13) of Fried[7], but with λ expressed in meters instead of microns. This quantity is set

equal to the diameter of the first Fresnel zone, to yield a condition for *Z*:

$$Z \le 9.4\lambda_\mu^{7/11}\left[\frac{10^{-16}}{C_n^2}\right]^{6/11} \text{ kilometers,} \qquad \text{(A33)}$$

where λ is again expressed in microns.

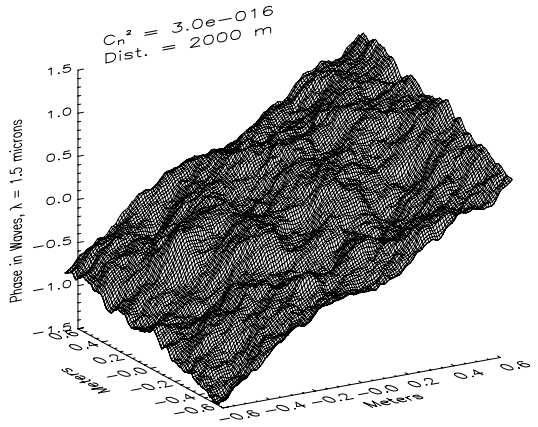

Figure A1. Typical phase screen. The overall tilt of the surface comes from the tilt term calculated in Sec. A3.

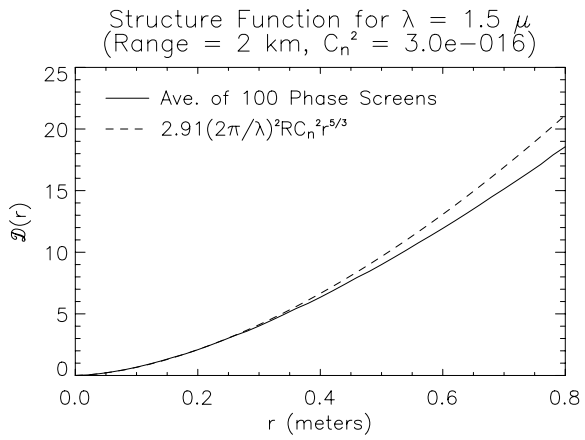

Figure A2. The structure function calculated statistically from the average of 100 phase screens similar to the screen of Fig. A1 (solid line) matches theory (dotted line) over region of interest here. A single screen does not affect amplitude, so the wave structure function and the phase structure function are identical.

REFERENCES

[1] R. L. Lucke and L. J Rickard, "Photon-limited synthetic-aperture imaging for planet surface studies", Applied Optics **41**, 5084 – 5095 (2002); erratum, Applied Optics **42**, 2766 (2002).

[2] J. C. Curlander and R. N. McDonough, *Synthetic Aperture Radar* (Wiley, New York, 1991).

[3] C. V. Jakowatz, D. E. Wahl, P. H. Eichel, D. C. Ghiglia and P. A. Thompson, *Spotlight-Mode Synthetic Aperture Radar* (Kluwer Academic Publishers, Norwell, Massachusetts 1996).

[4] M. Bashkansky, R. L. Lucke, E. Funk, L. J Rickard, J. Reintjes, Two-Dimensional Synthetic-Aperture Imaging in the Optical Domain", Opt. Lett. **27** (22), 1983 – 1985, 2002

[5] W. Buell, N. Marochal, R. P. Dickinson, D. A. Kozlowski, T. Wright, J. Buck, S. Beck, "Synthetic Aperture Imaging Ladar: Lab Demo & Signal Processing (U)", Military Sensing Symposium, Active Systems (F-4), V. 1, 2003.

[6] W. Buell, N. M. Marechal, R. P. Dickson, D. A. Kozlowski, S. Beck, "SAIL: Synthetic Aperture Imaging Ladar (U)", Military Sensing Symposium, Active Systems (C-15), V. 1, 2002.

[7] T. J. Karr, "Resolution of synthetic aperture imaging through turbulence", JOSA A **20**, 1067 - 1083 (2003).

[8] A. Belmonte and B. J. Ryle, "Heterodyne lidar returns in the turbulent atmosphere: performance evaluation of simulated systems", Applied Optics **39**, 2401 – 2411 (2000).

[9] D. L. Fried, "Optical Heterodyne Detection of an Atmospherically Distorted Signal Wave Front", Proceedings of the IEEE, **55**, 57 – 67 (1967).

[10] J. W. Goodman, *Introduction to Fourier Optics* (1st ed., McGraw-Hill, New York, 1988), Secs. 3-7, 6-2, 6-3.

[11] J. W. Goodman, *Statistical Optics* (Wiley, New York, 1985), p. 430.

[12] R. L. Lucke, "Fundamentals of Wide-Field Sparse-Aperture Imaging", 2001 IEEE Aerospace Conference Proceedings, Big Sky, Montana, March 10 - 17.

[13] R. L. Lucke and S. E. Thonnard, "Stacked-grid collimators described with dimensionless parameters", Applied Optics **37**, 616 - 621 (1998).

[14] R. L. Lucke, "The relation between physical and computer-generated PSFs and OTFs", Am. J. Phys. **69** (12), 1237 - 1244 (2001).

[15] S. F. Clifford, “The Classical Theory of Wave Propagation in a Turbulent Medium”, *Topics in Applied Physics*, Vol. 25, *Laser Beam Propagation in the Atmosphere* (J. W. Strohbehn, ed., Springer-Verlag, New York, 1978), pp. 9 - 43.

[16] R. G. Lane, A. Glindemann and J. C. Dainty, “Simulation of a Kolmogorov phase screen”, Waves in Random Media, **2** (1992) pp. 209 – 224.

Bob Lucke received his M. S. and Ph. D. degrees in physics from the Johns Hopkins University in 1971 and 1975, respectively. He has been at the Naval Research Laboratory since 1982, where he has worked in the areas of IR surveillance and satellite instrumentation, among others. He has applied theoretical and Fourier optics tools to the analysis of sparse aperture imaging and most recently to the analysis of synthetic aperture ladar.